Journal of Porous Media, 1(3), 227–241 (1998)

# Free Convection in a Shallow Annular Cavity Filled with a Porous Medium

**I. Pop,[1] D. A. S. Rees,[2] and L. Storesletten[3]**

[1]Faculty of Mathematics, University of Cluj,
R3400 Cluj, CP253, Romania
[2]School of Mechanical Engineering, University of Bath,
Claverton Down, Bath, BA2 7AY, United Kingdom
[3]Department of Mathematics, Agder College,
Tordenskjoldgate 65, 4604 Kristiansand, Norway

*Received September 16, 1996; Accepted April 9, 1997*

**ABSTRACT**

*In this paper, we consider free convection in a shallow annular cavity heated and cooled at the sidewalls and which is filled with a fluid-saturated porous medium. Attention is paid to the case where the aspect ratio, A, is asymptotically small. A combined asymptotic and numerical analysis of this flow is undertaken for Rayleigh numbers that are either $O(1)$ or $O(A^{-1})$ in magnitude. In both cases, there are three asymptotic regions within the cavity to be considered: a core flow and two endwall regions. When the Rayleigh number is $O(1)$ in magnitude, an analysis up to $O(A^4)$ is presented; it is found that core solutions at $O(A^n)$ are only determined precisely by considering the equations at $O(A^{n+2})$, and therefore, we obtained solutions up to $O(A^2)$. Successive solutions in the endwall regions are obtained as numerical solutions of Poisson's equation. When the Rayleigh number is $O(A^{-1})$ in magnitude, the leading-order core flow profile is modified and it depends on the Rayleigh number. The leading-order stream function and first-order temperature field in the endwall regions are given as the solution of a pair of coupled nonlinear partial differential equations. It is when the Rayleigh number is large within this order of magnitude that distinct boundary layers on the endwalls are generated. In both asymptotic regimes, expressions for the Nusselt number are derived.*

## NOMENCLATURE

| | |
|---|---|
| $A$ | aspect ratio, height-to-gap-width |
| $a$ | constant |
| $C_p$ | heat capacity |
| $c_1, \ldots, c_4$ | constants |
| $f(\hat{x})$, $g(\hat{x})$, $h(\hat{x})$, $k(\hat{x})$ | core functions |
| $g$ | gravitational acceleration |
| $h$ | cavity height |
| $K$ | permeability of the porous medium |
| $k$ | effective thermal conductivity |
| $Nu$ | Nusselt number |
| $Q$ | overall heat flux |
| $R$ | scaled Rayleigh number |
| $Ra$ | Rayleigh number |
| $r_c$, $r_h$ | cold and hot endwall radii |
| $\bar{r}$, $\phi$, $\bar{z}$ | cylindrical polar coordinates |
| $T$ | temperature |
| $T_c$, $T_h$ | cold and hot endwall temperatures |
| $\bar{u}$, $\bar{w}$ | radial and vertical velocity components |
| $x^*$ | cold endwall scaled radial variable |
| $x$, $z$ | nondimensional radial and vertical coordinates |

Greek symbols

| | |
|---|---|
| $\alpha$ | effective thermal diffusivity |
| $\beta$ | coefficient of thermal expansion |
| $\Delta T$ | temperature drop across the annulus, $T_h - T_c$ |
| $\delta$ | length-scale ratio |
| $\Theta$ | temperature function |
| $\theta$ | scaled temperature |
| $\nu$ | kinematic viscosity |
| $\rho$ | annulus aspect ratio |
| $\rho^*$ | reference fluid density |
| $\Phi$ | scaled stream function |
| $\psi$ | nondimensional stream function |

Subscripts

| | |
|---|---|
| $c$ | cold |
| $h$ | hot |
| $i$ | terms in asymptotic expansion |

Superscripts

| | |
|---|---|
| $\bar{}$ | dimensional variables |
| $\hat{}$ | core region variables |
| $'$ | differentiation with respect to $\hat{x}$ |

## INTRODUCTION

Heat transfer in porous media is of fundamental importance because of its many technological applications in geothermal energy utilization, insulation of high-temperature gas-cooled reactor vessels, the burying of drums containing heat-generating chemicals in the Earth, thermal energy storage tanks, petroleum reservoirs, and chemical catalytic convertors, etc. However, convective flow in a shallow, two-dimensional cavity filled with a porous medium has occupied center stage in many fundamental heat transfer analyses. One common method of maintaining convective flows has been to use externally supplied temperature gradients across the system. A great deal of research, both theoretical and experimental, on this classical heat transfer process has accumulated over the last three decades. Bejan (1987) and Nield and Bejan (1992) have presented detailed surveys on this topic.

In contrast, there is a marked paucity of studies of convective flow in a shallow "annular" cavity filled with a porous medium, although an understanding of this type of heat transfer process is essential because of its numerous applications in geophysics and energy-related problems. Examples of these applications include the insulation of pipes, the deep geological disposal of high-level nuclear waste, and thermal energy storage systems. In a proposed repository, a waste canister surrounded by crushed rock (the "engineered" barrier to radionuclide release) can be adequately modeled as a porous annulus.

The problem of free convection flow in a vertical porous annulus when the inner wall is heated and the outer wall cooled, and where the upper and lower surfaces are insulated, was considered by Hickox and Gartling (1985). Using a finite element technique, they obtained heat transfer results for Rayleigh numbers up to 100. The range of aspect ratio they considered was $2 \leq A \leq 8$. They also developed an approximate analytical method valid for low Rayleigh numbers and high aspect ratios.

Havstad and Burns (1982) used three different methods, a finite difference computation, an asymptotic technique, and a perturbation analysis to study free convection in a vertical annular cavity filled with a porous medium. Of these methods, only the first two were used to obtain heat transfer results, whereas the third was used to establish the temperature and velocity fields for low Rayleigh numbers. These authors have correlated their results with a five-constant empirical formula valid for low Rayleigh numbers. In the boundary-layer regime at high Rayleigh numbers, Bejan (1984) has proposed, using scale analysis, a simpler two-constant correlation equation.

More recently, Prasad and Kulacki (1984, 1985) and Prasad et al. (1986), using comprehensive numerical and experimental studies, have extended the results of Hickox and Gartling (1985) and Havstad and Burns (1982) to Rayleigh numbers as high as $10^4$. They have investigated both the boundary-layer and curvature effects that arise in the presence of strongly convecting flow. It was shown that the flow patterns and the isotherms are affected significantly by curvature. Correlation equations for critical Rayleigh numbers were also proposed to delimit the various flow regimes. Other works in this general area include a study of the effects of internal heating (Rao and Wang 1991) and the effects of departures from Darcy's law (Dharma Rao et al., 1996).

Notwithstanding the preceding review of the topic, further work is needed to improve our understanding of flow in a porous annulus. This paper deals with the case where the aspect ratio, as just defined, is asymptotically small and, therefore, the annulus is very shallow. There is an overall temperature drop from the inner to the outer surfaces, and the upper and lower surfaces are again insulated. In this regard, we are considering the porous medium analogue of the clear fluid problem considered by Merker and Leal (1980). However, we do not follow their methodology, but use the classical method of matched asymptotic expansions to obtain solutions in the end regions (i.e., near the vertical walls), and in the core (far from the endwalls). The use of this method obviates the necessity of making assumptions about the form of the flow in the core at leading order. In this paper, we not only present the porous medium analogue of the Merker and Leal (1980) analysis, for which we take $Ra = O(1)$, but also extend it to asymptotically large values [$Ra = O(A^{-1})$]. It is within this latter regime that boundary layers first begin to form on the vertical sidewalls. At still higher Rayleigh numbers, the present solution methodology breaks down and the asymptotic analysis is very different because the boundary layers on the vertical surfaces dominate the flow; such a study is outside the scope of the present paper.

## GOVERNING EQUATIONS

We consider a closed annular cavity with inner radius $r_h$, outer radius $r_c$, and height $h$, as shown in Fig. 1. The cavity is filled with a fluid-saturated porous medium, and the inner and outer walls are held at different but uniform temperatures, $T_h$ and $T_c$, respectively, with $T_h > T_c$. The top and bottom surfaces are insulated, and all surfaces are rigid and impermeable.

It is convenient to introduce cylindrical polar coordinates, $(\bar{r}, \phi, \bar{z})$, and their corresponding velocity components, $(\bar{u}, \bar{v}, \bar{w})$. In the problem we consider, there is no reason to expect the flow to be anything other than axisymmetric and two dimensional, al-

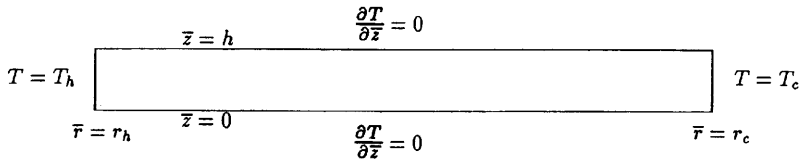


**Figure 1.** Basic flow configuration, a shallow annular cavity filled with a porous medium, subjected to a radial flow of heat, with the upper and lower surfaces insulated.

though we note that the flow at very high Rayleigh numbers may exhibit three-dimensional instabilities. Therefore, we take $\bar{v} = 0$ and neglect all $\phi$ derivatives. Assuming that Darcy's law and the Boussinesq approximation are both valid, the governing equations for steady convective flow can be written as

$$\frac{\partial}{\partial \bar{r}}(\bar{r}\bar{u}) + \frac{\partial}{\partial \bar{z}}(\bar{r}\bar{w}) = 0 \tag{1}$$

$$\frac{\partial \bar{u}}{\partial \bar{z}} - \frac{\partial \bar{w}}{\partial \bar{r}} = -\frac{gK\beta}{\nu}\frac{\partial T}{\partial \bar{r}} \tag{2}$$

$$\bar{u}\frac{\partial T}{\partial \bar{r}} + \bar{w}\frac{\partial T}{\partial \bar{z}} = \alpha\left[\frac{1}{\bar{r}}\frac{\partial}{\partial \bar{r}}\left(\bar{r}\frac{\partial T}{\partial \bar{r}}\right) + \frac{\partial^2 T}{\partial \bar{z}^2}\right] \tag{3}$$

see Prasad and Kulacki (1984). We introduce a stream function using

$$\bar{u} = -\frac{1}{\bar{r}}\frac{\partial \bar{\psi}}{\partial \bar{z}}, \quad \bar{w} = \frac{1}{\bar{r}}\frac{\partial \bar{\psi}}{\partial \bar{r}} \tag{4}$$

and nondimensionalize by setting

$$x = (\bar{r} - r_h)/h, \quad z = \bar{z}/h \tag{5}$$

$$\psi = \bar{\psi}/(h\alpha Ra), \quad \theta = (T - T_c)/(T_h - T_c) \tag{6}$$

Three (mutually dependent) aspect ratios are defined according to

$$A = h/(r_c - r_h), \quad \delta = r_h/h, \quad \rho = A\delta = r_h/(r_c - r_h) \tag{7}$$

and the Rayleigh number for convective flow in porous media is defined as

$$Ra = \frac{gK\beta(T_h - T_c)h}{\alpha\nu} \tag{8}$$

On substituting these definitions into momentum and energy Eqs. (2) and (3), we obtain the following governing equations:

$$\frac{A}{(\rho + Ax)}\nabla^2\psi - \frac{A^2}{(\rho + Ax)^2}\frac{\partial \psi}{\partial x} = \frac{\partial \theta}{\partial x} \tag{9}$$

$$\nabla^2\theta + \frac{A}{(\rho + Ax)}\frac{\partial \theta}{\partial x} = Ra\frac{A}{(\rho + Ax)}\left(\frac{\partial \psi}{\partial x}\frac{\partial \theta}{\partial z} - \frac{\partial \psi}{\partial z}\frac{\partial \theta}{\partial x}\right) \tag{10}$$

subject to the boundary conditions

$$\psi = \frac{\partial \theta}{\partial z} = 0 \quad \text{at} \quad z = 0, 1 \tag{11}$$

$$\psi = 0, \quad \theta = 1 - Ax \quad \text{at} \quad x = 0, A^{-1} \tag{12}$$

and where the Laplacian operator used in Eqs. (9) and (10) is defined as

$$\nabla^2 = \frac{\partial^2}{\partial x^2} + \frac{\partial^2}{\partial z^2} \tag{13}$$

We seek solutions of Eqs. (9)–(12) for arbitrary values of $Ra$ in the shallow layer limit, i.e., $A \to 0$. There are two different cases of interest as $A \to 0$, namely, $\rho = O(1)$ and $\delta = O(1)$. The former case corresponds to annuli where the inner radius is asymptotically larger than the annulus depth, $h$, whereas the latter case has the inner radius and layer depth of the same order of magnitude. In the present work, we shall restrict attention solely to the former case.

The equations of motion are solved using the method of matched asymptotic expansions, and it is shown that the flow divides into three distinct regions corresponding to a nearly parallel core flow in the main body of the annulus, and two nonparallel turning regions near the heated and cooled endwalls. Although the flow configuration considered here is identical to that of Merker and Leal's (1980) analysis of a Newtonian fluid, we do not assume that the core flow is parallel at leading order, but prove that it is by rigorous analytical means using a solvability condition at second order in the asymptotic expansion.

## Equations of Motion in the Core Region

Governing Eqs. (9) and (10) may be expressed in a form that is more appropriate for the core region because the horizontal length scale in the cavity is much greater than the vertical scale. Thus, it is convenient to rescale the equations according to

$$\hat{x} = Ax, \quad \hat{\psi} = \psi, \quad \hat{\theta} = \theta \tag{14}$$

which leads to

$$A^2\frac{\partial^2 \hat{\psi}}{\partial \hat{x}^2} + \frac{\partial^2 \hat{\psi}}{\partial z^2} - \frac{A^2}{(\rho + \hat{x})}\frac{\partial \hat{\psi}}{\partial \hat{x}} = (\rho + \hat{x})\frac{\partial \hat{\theta}}{\partial \hat{x}} \tag{15}$$

$$A^2\frac{\partial^2 \hat{\theta}}{\partial \hat{x}^2} + \frac{\partial^2 \hat{\theta}}{\partial z^2} + \frac{A^2}{(\rho + \hat{x})}\frac{\partial \hat{\theta}}{\partial \hat{x}} = Ra\frac{A^2}{\rho + \hat{x}}\left(\frac{\partial \hat{\psi}}{\partial \hat{x}}\frac{\partial \hat{\theta}}{\partial z} - \frac{\partial \hat{\psi}}{\partial z}\frac{\partial \hat{\theta}}{\partial \hat{x}}\right) \tag{16}$$

Here, $\hat{x}$ and $\rho$ are both $O(1)$ quantities as $A \to 0$. In the core region we seek solutions in the form of the asymptotic expansion

$$(\hat{\psi}, \hat{\theta}) = \sum_{n=0}^{\infty} A^n(\hat{\psi}_n, \hat{\theta}_n) \tag{17}$$

### Equations of Motion in the End Regions

In the end regions, the characteristic horizontal length-scale turns out to be $O(h)$, dimensionally, and this has already been assumed when obtaining Eqs. (9) and (10). Thus, we seek solutions of Eqs. (9) and (10) in the same form as Eq. (17), where the variables $\hat{\psi}$ and $\hat{\theta}$ are replaced by $\psi$ and $\theta$.

## ASYMPTOTIC ANALYSIS FOR $Ra = O(1)$

In this section, we consider in detail the case $Ra = O(1)$ and present an asymptotic expansion valid in the core and end regions of the cavity. These solutions are matched asymptotically using the matching principles

$$\lim_{\hat{x}\to 0}(\hat{\psi}, \hat{\theta})_{\text{core}} \sim \lim_{x\to\infty}(\psi, \theta)_{\text{hot end}} \quad \text{as} \quad A \to 0 \tag{18}$$

$$\lim_{\hat{x}\to 1}(\hat{\psi}, \hat{\theta})_{\text{core}} \sim \lim_{x^*\to -\infty}(\psi, \theta)_{\text{cold end}} \quad \text{as} \quad A \to 0 \tag{19}$$

where $x^* = x - A^{-1}$ is the appropriate horizontal variable in the cold-end region.

### Solutions at $O(1)$

Although the flow is generated by means of differential heating along the length of the cavity, and the fluid motion would seem to be initiated at the ends of the cavity, it turns out that at this order of magnitude of the Rayleigh number, it is necessary to consider first the flow in the core region before turning to that in the end regions. At leading order in the core the equations are

$$\frac{\partial^2 \hat{\psi}_0}{\partial z^2} = (\rho + \hat{x})\frac{\partial \hat{\theta}_0}{\partial \hat{x}} \tag{20}$$

$$\frac{\partial^2 \hat{\theta}_0}{\partial z^2} = 0 \tag{21}$$

subject to the boundary conditions [Eq. (11)]. The integration of Eq. (21) and satisfaction of the appropriate boundary conditions gives

$$\hat{\theta}_0 = f(\hat{x}) \tag{22}$$

where $f(\hat{x})$ is at present an arbitrary function. Following this, the leading-order stream function is given by

$$\hat{\psi}_0 = (\rho + \hat{x})f'(\hat{x})\frac{(z^2 - z)}{2} \tag{23}$$

where the prime denotes differentiation with respect to $\hat{x}$. It is at this stage that Merker and Leal (1980) assume that the leading-order flow in the core is parallel and insist that $\hat{\psi}_0$ is independent of $\hat{x}$. Although it turns out that this assumption is indeed correct for the present problem, we shall not specify $f(\hat{x})$ at this point, but leave it arbitrary at this stage of the analysis. At $O(A^2)$, we find that the governing equations in the core cannot be solved unless $f(\hat{x})$ takes a specific form.

From Eqs. (9) and (10), we obtain the following leading-order equations that are valid in the end regions:

$$\frac{\partial \theta_0}{\partial x} = 0, \quad \nabla^2 \theta_0 = 0 \tag{24}$$

The solutions of these equations, which are compatible with boundary conditions (11) and (12), give the following values for $\theta_0$ in the end regions:

$$\text{hot end:} \quad \theta_0 = 1 \tag{25}$$

$$\text{cold end:} \quad \theta_0 = 0 \tag{26}$$

These solutions must match those of the core solution, and if we write Eq. (22) as a Taylor-series expansion in $\hat{x}$

$$\hat{\theta} = f(\hat{x}) = f(0) + \hat{x}f'(0) + \frac{1}{2}\hat{x}^2 f''(0) + \cdots$$

it then becomes

$$\hat{\theta} = f(0) + Axf'(0) + \cdots$$

when rewritten in terms of the hot end region variable, $x$. Applying the matching relation [Eq. (18)], at the hot end

$$\theta_0 + A\theta_1 + \cdots + \sim f(0) + Axf'(0) + \cdots \quad \text{as} \quad A \to 0,$$

we obtain

$$f(0) = 1 \tag{27}$$

In similar fashion we show that the cold endwall boundary condition is

$$f(1) = 0 \tag{28}$$

### Solutions at $O(A)$

In the core region, the governing equations at $O(A)$ are identical to the leading-order equations, Eqs. (20) and (21), except that the subscript 0 is replaced by 1. Thus, the core solution is

$$\hat{\theta}_1 = g(\hat{x}) \tag{29}$$

$$\hat{\psi}_1 = (\rho + \hat{x})g'(\hat{x})\frac{(z^2 - z)}{2} \tag{30}$$

where $g(\hat{x})$ is to be determined later, at $O(A^3)$. Equation (10), when expanded in powers of $A$, yields the following equation for $\theta_1$ at $O(A)$:

$$\nabla^2\theta_1 = 0 \tag{31}$$

which is to be solved subject to the boundary conditions

$$\frac{\partial\theta_1}{\partial z} = 0 \quad \text{at} \quad z = 0, 1 \quad \text{and} \quad \theta_1 = 0 \quad \text{at} \quad x = 0 \tag{32}$$

Equations (31) and (32) have the solution $\theta_1 = c_1 x$, where the constant $c_1$ is found by matching with the core solution:

$$\hat{\theta} = \hat{\theta}_0 + A\hat{\theta}_1 + \cdots + = f(\hat{x}) + Ag(\hat{x}) + \cdots = f(0) + A[xf'(0) + g(0)] + \cdots \tag{33}$$

It follows that

$$c_1 = f'(0) \quad \text{and} \quad g(0) = 0 \tag{34}$$

and, similarly in the cold-end region. Thus, the respective solutions in the hot and cold ends are

$$\theta_1 = f'(0)x \quad \text{and} \quad \theta_1 = f'(1)x^* \tag{35}$$

The equation for $\psi_0$ is

$$\nabla^2\psi_0 = \rho\frac{\partial\theta_1}{\partial x} = \rho f'(0) \equiv a \tag{36}$$

which is solved subject to the boundary conditions

$$\psi_0 = 0 \quad \text{at} \quad z = 0, 1; \quad \psi_0 = 0 \quad \text{at} \quad x = 0; \quad \psi_0 \quad \text{is finite as} \quad x \to \infty \tag{37}$$

where $a$, defined by Eq. (36), is as yet unknown. Equation (36) and boundary conditions (37) are equivalent to the problem of flow along a large-aspect-ratio, two-dimensional duct. The solution is easily obtained numerically using a pointwise Gauss-Seidel iteration scheme with multigrid acceleration. The particular multigrid method used was a standard Correction Scheme approach, as described in Brandt (1984), with a pointwise Gauss-Seidel iteration. Convergence was deemed to have taken place when the residuals were less than $10^{-8}$. A $128 \times 32$ grid was used on a computational region with aspect ratio 4; such a grid, in combination with a second-order accurate finite difference discretization, yields very accurate results. The streamlines obtained from the use of this code are depicted in Fig. 2. The solution may also be written analytically as

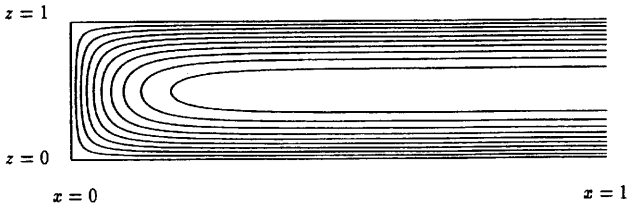


**Figure 2.** Basic streamlines corresponding to $\psi_0$ given by Eq. (38).

$$\psi_0 = a\left[\frac{z^2 - z}{2} + \frac{4}{\pi^3}\sum_{m=1}^{\infty}\frac{1}{(2m-1)^3} \cdot \exp[-(2m-1)\pi x]\sin(2m-1)\pi z\right] \tag{38}$$

or, for later reference, as

$$\psi_0 = a\left[\frac{z^2 - z}{2} + \Phi(x, z)\right] \tag{39}$$

where the function $\Phi(x, z)$ is defined by direct comparison with Eq. (38). Near the cold end wall, $\hat{x} \sim 1$, the stream function is given by

$$\psi_0 = a\left[\frac{z^2 - z}{2} + \Phi(-x^*, z)\right] \tag{40}$$

### Solutions at $O(A^2)$

It follows from Eqs. (16), (22), and (23) that

$$\frac{\partial^2\hat{\theta}_2}{\partial z^2} = -\left(f'' + \frac{f'}{\rho + \hat{x}}\right) - Raf'f'\left(z - \frac{1}{2}\right) \tag{41}$$

Integrating once with respect to $z$ gives

$$\frac{\partial\hat{\theta}_2}{\partial z} = -\left(f'' + \frac{f'}{\rho + \hat{x}}\right)z - Raf'f'\left(\frac{z^2 - z}{2}\right) + c_2(\hat{x}) \tag{42}$$

The insulating boundary conditions at $z = 0$ and 1 imply that $c_2(\hat{x}) = 0$, and that

$$f'' + \frac{f'}{\rho + \hat{x}} = 0 \tag{43}$$

The solution of Eq. (43) together with the boundary conditions, (27) and (28), which were derived earlier, is

$$f(\hat{x}) = a \ln\left(\frac{\rho + \hat{x}}{\rho + 1}\right) \tag{44a}$$

where $a$ is now found to be

$$a = \left(\ln\frac{\rho}{\rho + 1}\right)^{-1} \tag{44b}$$

Consequently, the core solutions at $O(1)$ are, precisely

$$\hat{\psi}_0 = a\left(\frac{z^2 - z}{2}\right), \quad \hat{\theta}_0 = a \ln\left(\frac{\rho + \hat{x}}{\rho + 1}\right) \tag{45}$$

From this, we see that the core flow is parallel at leading order, but this result has been proved rigorously rather than having been assumed at the outset. Integrating Eq. (42) once more yields

$$\hat{\theta}_2 = -Raf'f'\left(\frac{z^3}{6} - \frac{z^2}{4} + \frac{1}{24}\right) + h(\hat{x}), \tag{46}$$

where $h(\hat{x})$ will be determined at $O(A^4)$. We introduced the constant, 1/24, into the polynomial part of Eq. (46); this is simply to make that part of the solution odd about $z = 1/2$, and such an approach is allowable because $h(\hat{x})$ remains arbitrary at this point in the analysis. The equation for $\hat{\psi}_2$ is found from using Eq. (46) in Eq. (15), and it is

$$\frac{\partial^2\hat{\psi}_2}{\partial z^2} = (\rho + \hat{x})h' - Ra(\rho + \hat{x})f'f'' \cdot\left(\frac{z^3}{3} - \frac{z^2}{2} + \frac{1}{12}\right) \tag{47}$$

for which the solution is

$$\hat{\psi}_2 = (\rho + \hat{x})h'(\hat{x})\left(\frac{z^2 - z}{2}\right) - Ra(\rho + \hat{x})f'f''\left(\frac{z^5}{60} - \frac{z^4}{24} + \frac{z^2}{24} - \frac{z}{60}\right) \tag{48}$$

In the hot end region, it follows from Eq. (10) that

$$\nabla^2\theta_2 = -\frac{a}{\rho} - Ra\frac{a}{\rho^2}\frac{\partial\psi_0}{\partial z} \tag{49}$$

where $\psi_0$ is given in Eq. (39). It is possible to write down the solution to this equation, when subject to the insulating boundary conditions at $z = 0$ and 1, and with $\theta_2 = 0$ at $x = 0$, in the following form:

$$\theta_2 = -\frac{a}{2\rho^2}x^2 + c_3x - Ra\frac{a^2}{\rho^2}\Theta \tag{50}$$

where the constant $c_3$ is found by matching, and the function $\Theta$ satisfies the equation

$$\nabla^2\Theta = z - \frac{1}{2} + \frac{\partial\Phi}{\partial z} \tag{51}$$

and the boundary conditions

$$\frac{\partial\Theta}{\partial z} = 0 \quad \text{at} \quad z = 0, 1, \quad \Theta = 0 \quad \text{at} \quad x = 0$$
$$\text{and} \quad \frac{\partial\Theta}{\partial x} \to 0 \quad \text{as} \quad x \to \infty \tag{52}$$

Equation (51) was solved numerically using the same pointwise Gauss-Seidel/multigrid Poisson solver, and the isotherms corresponding to $\Theta$ are shown in Fig. 3.

Solutions (46) and (50) must now satisfy the matching condition (18). As

$$\begin{aligned}\hat{\theta} &= \hat{\theta}_0 + A\hat{\theta}_1 + A^2\hat{\theta}_2 + \cdots \\ &= 1 + A[xf'(0) + g(0)] + A^2\left[\frac{1}{2}x^2f''(0) + xg'(0) + h(0) - Raf'(0)f'(0) \cdot\left(\frac{z^3}{6} - \frac{z^2}{4} + \frac{1}{24}\right)\right] + \cdots\end{aligned} \tag{53}$$

for small values of $\hat{x}$, it follows that

$$-\frac{a^2}{2\rho^2}x^2 + c_3x - Ra\frac{a^2}{\rho^2}\Theta \sim \frac{1}{2}x^2f''(0) + xg'(0) + h(0) - Raf'(0)f'(0) \cdot\left(\frac{z^3}{6} - \frac{z^2}{4} + \frac{1}{24}\right) = -\frac{a^2}{2\rho^2}x^2 + xg'(0) + h(0) - Ra\frac{a^2}{\rho^2}\left(\frac{z^3}{6} - \frac{z^2}{4} + \frac{1}{24}\right) \tag{54}$$

as $x \to \infty$. Because

$$\lim_{x\to\infty}\Theta = \frac{z^3}{6} - \frac{z^2}{4} + \frac{1}{24}$$

the matching is consistent if $c_3 = g'(0)$ and $h(0) = 0$. Similarly, we find that $h(1) = 0$. Thus, we obtain

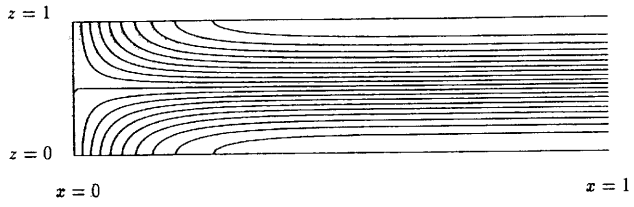


**Figure 3.** Isotherms corresponding to the function $\Theta$ given by Eq. (51).

$$\theta_2 = -\frac{a^2}{2\rho^2}x^2 + g'(0)x - Ra\frac{a^2}{\rho^2}\Theta \tag{55}$$

The equation governing $\psi_1$ is obtained from Eq. (9) at second order in $A$, and is

$$\nabla^2\psi_1 = \frac{a}{\rho}\frac{\partial\Phi}{\partial x} - Ra\frac{a^2}{\rho}\frac{\partial\Theta}{\partial x} + \rho g'(0) \tag{56}$$

in the hot end region. Because the $x$ derivatives on the right-hand side of Eq. (56) tend to zero as $x \to \infty$, it follows that

$$\psi_1 \to \rho g'(0)\frac{(z^2 - z)}{2} \quad \text{as} \quad x \to \infty \tag{57}$$

The detailed solution for $\psi_1$ is found numerically using the program described earlier, but we will not present results because they now depend on the precise value of $Ra$. Matching with the core flow also gives consistent results.

### Solutions at $O(A^3)$

The equation for $\hat{\theta}_3$ is given by

$$\frac{\partial^2\hat{\theta}_3}{\partial z^2} + g'' + \frac{g'}{(\rho + \hat{x})} = -Raf'g'\left(z - \frac{1}{2}\right) \tag{58}$$

Integration once with respect to $z$, and the application of the boundary conditions at $z = 0$ and 1, yields the following equation:

$$g'' + \frac{g'}{(\rho + \hat{x})} = 0 \tag{59}$$

We have shown that $g(0) = g(1) = 0$ are the boundary conditions and, therefore, we conclude that $g(\hat{x}) = 0$. It follows that the $O(A)$ core solutions, (29) and (30), are

$$\hat{\theta}_1 = 0, \quad \hat{\psi}_1 = 0 \tag{60}$$

The core solutions at $O(A^3)$ now take the following form:

$$\hat{\theta}_3 = k(\hat{x}), \quad \hat{\psi}_3 = (\rho + \hat{x})k'(\hat{x})\frac{(z^2 - z)}{2} \tag{61}$$

where $k(\hat{x})$ is determined at fifth order.

Given that the core solutions at $O(A)$ are zero, it is necessary to go to $O(A^4)$ in the present analysis to determine the leading correction [i.e., the $O(A^2)$ terms] to the parallel core flow profile.

The end region solutions at $O(A^3)$ are more complicated than those at lower orders, but their determination is straightforward as it only involves the solution of two uncoupled Poisson equations. More importantly, we note that these solutions do not affect the $O(A^4)$ core solutions that we now consider.

### Solutions at $O(A^4)$

The determination of the unknown function, $h(\hat{x})$, which appears in the $O(A^2)$ core solutions, requires us to consider the solution for $\hat{\theta}_4$. The equation for $\hat{\theta}_4$ may be shown to be given by

$$\begin{aligned}\frac{\partial^2\hat{\theta}_4}{\partial z^2} = &-\left(h'' + \frac{h'}{\rho + \hat{x}}\right) \\ &+ Ra\left(\frac{f'f''}{\rho + \hat{x}} + f'f''' + f''f''\right) \\ &\cdot\left(\frac{z^3}{3} - \frac{z^2}{2} + \frac{1}{12}\right) - Ra(2z - 1)f'h' \\ &+ Ra^2f'f'f''\left(\frac{5z^4}{12} - \frac{5z^3}{6} + \frac{z^2}{4} + \frac{z}{12} - \frac{1}{60}\right)\end{aligned} \tag{62}$$

Integrating Eq. (62) with respect to $z$, and applying the boundary conditions at $z = 0$ and 1, lead to the following equation for $h$:

$$h'' + \frac{h'}{\rho + \hat{x}} + \frac{1}{60}Ra^2f'f'f'' = 0 \tag{63}$$

The solution of this equation subject to the boundary conditions, $h(0) = h(1) = 0$, is

$$\begin{aligned}h(\hat{x}) = \frac{Ra^2a^3}{240}\Bigg(&\frac{1}{(\rho + \hat{x})^2} - \frac{1}{\rho^2} \\ &- \frac{a(2\rho + 1)}{\rho^2(\rho + 1)^2}\ln\frac{\rho}{\rho + \hat{x}}\Bigg)\end{aligned} \tag{64}$$

Having found Eq. (64), it is straightforward to write down $\hat{\psi}_2$ and $\hat{\theta}_2$, using Eqs. (46) and (48), although the resulting expressions are lengthy. It is clear from

Eq. (48) that the core flow is not parallel at this order in the expansion as $\hat{\psi}_2$ is a function of $\hat{x}$.

## ASYMPTOTIC ANALYSIS FOR $Ra = O(A^{-1})$

The asymptotic analysis carried out in the preceding Asymptotic Analysis for $Ra = O(1)$ section was for the $Ra = O(1)$ case. A detailed consideration of the magnitudes of the various terms in the asymptotic expansion shows that it is also valid if $Ra = o(A^{-1})$, i.e., if $RaA \ll 1$ as $A \to 0$. The core solutions at $O(A^2)$ given in Eqs. (46) and (48) contain terms that are proportional to $Ra^2$, and therefore, these "second-order" solutions are formally the same order of magnitude as the $O(1)$ solutions, when $Ra = O(A^{-1})$. Therefore, we would expect the leading-order core profile to be modified at such large values of the Rayleigh number.

In this section, we develop an analysis that is valid when $Ra = O(A^{-1})$. A rescaled Rayleigh number, $R$, is introduced by setting

$$R = RaA \tag{65}$$

Energy Eqs. (10) and (16) become

$$\nabla^2\theta + \frac{A}{(\rho + Ax)}\frac{\partial\theta}{\partial x} = \frac{R}{(\rho + Ax)}\left(\frac{\partial\psi}{\partial x}\frac{\partial\theta}{\partial z} - \frac{\partial\psi}{\partial z}\frac{\partial\theta}{\partial x}\right) \tag{66}$$

$$A^2\frac{\partial^2\hat{\theta}}{\partial\hat{x}^2} + \frac{\partial^2\hat{\theta}}{\partial z^2} + \frac{A^2}{(\rho + \hat{x})}\frac{\partial\hat{\theta}}{\partial\hat{x}} = \frac{RA}{(\rho + \hat{x}}\left(\frac{\partial\hat{\psi}}{\partial\hat{x}}\frac{\partial\hat{\theta}}{\partial z} - \frac{\partial\hat{\psi}}{\partial z}\frac{\partial\hat{\theta}}{\partial\hat{x}}\right) \tag{67}$$

while the equations for stream function (9) and (15) are unchanged. We seek asymptotic core solutions of Eqs. (15) and (67), and end-region solutions of Eqs. (9) and (66) in the same form as expansion (17).

### Solutions at $O(1)$

Leading-order equations in the core are identical to Eqs. (20) and (21), and the solutions are

$$\hat{\psi}_0 = (\rho + \hat{x})f'(\hat{x})\frac{(z^2 - z)}{2}, \quad \hat{\theta}_0 = f(\hat{x}) \tag{68}$$

where the function $f(\hat{x})$ is to be determined at $O(A^2)$. Note that $f(\hat{x})$ will be different from that found in the Asymptotic Analysis for $Ra = O(1)$ section, and which was given by Eq. (43). From Eqs. (9) and (66), we obtain the leading-order equations valid in the end regions. The solutions are once again given by

$$\text{hot end:} \quad \theta_0 = 1, \qquad \text{cold end:} \quad \theta_0 = 0 \tag{69}$$

Matching with the core solutions yields

$$f(0) = 1, \quad f(1) = 0 \tag{70}$$

### Solutions at $O(A)$

In the core region, the governing equations at $O(A)$ are

$$\frac{\partial^2\hat{\psi}_1}{\partial z^2} = (\rho + \hat{x})\frac{\partial\hat{\theta}_1}{\partial\hat{x}} \tag{71}$$

$$\frac{\partial^2\hat{\theta}_1}{\partial z^2} = -Rf'f'\left(z - \frac{1}{2}\right) \tag{72}$$

Integration twice with respect to $z$, and the application of the boundary conditions at $z = 0$ and 1, leads to

$$\hat{\theta}_1 = g(\hat{x}) - Rf'f'\left(\frac{z^3}{6} - \frac{z^2}{4} + \frac{1}{24}\right) \tag{73}$$

where $g(\hat{x})$ may be determined later at $O(A^3)$, although we shall not proceed this far in our analysis. From Eqs. (71) and (73), we obtain

$$\hat{\psi}_1 = (\rho + \hat{x})\left[g'(\hat{x})\frac{(z^2 - z)}{2} - Rf'f'\left(\frac{z^5}{60} - \frac{z^4}{24} + \frac{z^2}{24} - \frac{z}{60}\right)\right] \tag{74}$$

In the hot end region, the governing equations at $O(A)$ are

$$\nabla^2\psi_0 = \rho\frac{\partial\theta_1}{\partial x} \tag{75}$$

$$\nabla^2\theta_1 = \frac{R}{\rho}\left(\frac{\partial\psi_0}{\partial x}\frac{\partial\theta_1}{\partial z} - \frac{\partial\psi_0}{\partial z}\frac{\partial\theta_1}{\partial x}\right) \tag{76}$$

where Eq. (69) has been used. The solutions have to match boundary conditions (32) and (37). Matching the core solutions, we obtain

$$\psi_0 \to \rho f'(0)\frac{(z^2 - z)}{2} \quad \text{as} \quad x \to \infty \tag{77}$$

$$\theta_1 \to g(0) + xf'(0) - Rf'(0)f'(0)\cdot\left(\frac{z^3}{6} - \frac{z^2}{4} + \frac{1}{24}\right) \quad \text{as} \quad x \to \infty \tag{78}$$

which, in turn, implies that

$$\frac{\partial \theta_1}{\partial x} \to f'(0) \quad \text{as} \quad x \to \infty$$

Equations (75) and (76) form a pair of coupled nonlinear partial differential equations that have to be solved numerically. A much more convenient form for the numerical work results from the following substitutions:

$$\psi_0 = \rho f'(0)\tilde{\psi}_0, \quad \theta_1 = f'(0)[\tilde{\theta}_1 + x],$$
$$R = -f'(0)\tilde{R} \tag{79}$$

which, when substituted into Eqs. (75) and (76), yields the following equations:

$$\nabla^2 \tilde{\psi}_0 = \frac{\partial \tilde{\theta}_1}{\partial x} + 1 \tag{80}$$

$$\nabla^2 \tilde{\theta}_1 = \tilde{R}\left[\frac{\partial \tilde{\psi}_0}{\partial x}\frac{\partial \tilde{\theta}_1}{\partial z} - \frac{\partial \tilde{\psi}_0}{\partial z}\frac{\partial \tilde{\theta}_1}{\partial x}\right] r - \tilde{R}\frac{\partial \tilde{\psi}_0}{\partial z} \tag{81}$$

subject to the boundary conditions

$$z = 0, 1: \quad \tilde{\psi}_0 = 0, \quad \frac{\partial \tilde{\theta}_1}{\partial z} = 0 \tag{82}$$

$$x = 0: \quad \tilde{\psi}_0 = 0, \quad \tilde{\theta}_1 = 0 \tag{83}$$

$$x \to \infty: \quad \frac{\partial \tilde{\psi}_0}{\partial x} \to 0, \quad \frac{\partial \tilde{\theta}_1}{\partial x} \to 0 \tag{84}$$

The number of parameters has been reduced from two

***Table 1***

*Values of $f'(0)$ for various values of $R$ and $\rho$*

| $R$ | $\rho = 0.01$ | $\rho = 0.1$ | $\rho = 1$ | $\rho = 10$ |
|---|---|---|---|---|
| 1 | −21.7081 | −4.1703 | −1.4427 | −1.0492 |
| 1 | −11.6859 | −3.8188 | −1.4317 | −1.0484 |
| 2 | −8.4655 | −3.3230 | −1.4038 | −1.0461 |
| 5 | −5.4773 | −2.4985 | −1.3027 | −1.0362 |
| 10 | −4.1478 | −2.0279 | −1.2096 | −1.0255 |
| 20 | −3.5148 | −1.7955 | −1.1585 | −1.0192 |
| 50 | −3.2748 | −1.7078 | −1.1390 | −1.0167 |
| 100 | −3.2371 | −1.6941 | −1.1360 | −1.0164 |
| 200 | −3.2275 | −1.6906 | −1.1352 | −1.0163 |
| 500 | −3.2248 | −1.6896 | −1.1350 | −1.0162 |
| 1000 | −3.2244 | −1.6895 | −1.1350 | −1.0162 |
| ∞ | −3.2243 | −1.6894 | −1.1349 | −1.0162 |

***Table 2***

*Values of $f'(1)$ for various values of $R$ and $\rho$*

| $R$ | $\rho = 0.01$ | $\rho = 0.1$ | $\rho = 1$ | $\rho = 10$ |
|---|---|---|---|---|
| 1 | −0.2149 | −0.3791 | −0.7213 | −0.9538 |
| 1 | −0.2469 | −0.3889 | −0.7249 | −0.9545 |
| 2 | −0.2828 | −0.4110 | −0.7348 | −0.9565 |
| 5 | −0.3810 | −0.4969 | −0.7820 | −0.9654 |
| 10 | −0.5150 | −0.6187 | −0.8430 | −0.9755 |
| 20 | −0.6304 | −0.7123 | −0.8822 | −0.9816 |
| 50 | −0.6812 | −0.7514 | −0.8976 | −0.9840 |
| 100 | −0.6892 | −0.7576 | −0.9000 | −0.9843 |
| 200 | −0.6913 | −0.7591 | −0.9006 | −0.9844 |
| 500 | −0.6919 | −0.7596 | −0.9008 | −0.9844 |
| 1000 | −0.6920 | −0.7596 | −0.9008 | −0.9844 |
| ∞ | −0.6920 | −0.7596 | −0.9008 | −0.9844 |

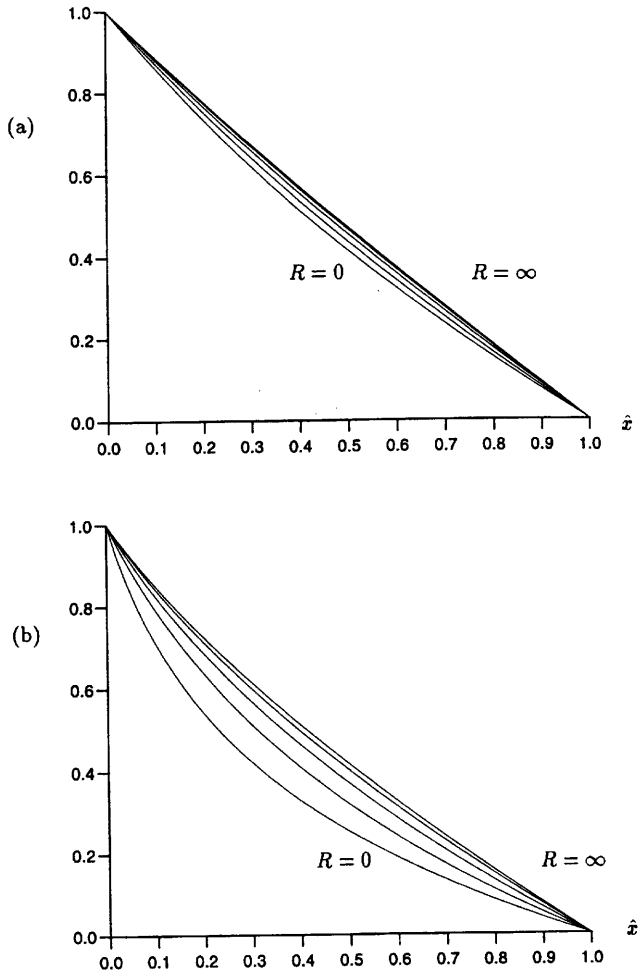


**Figure 4.** Profiles of the core function, $f(\hat{x})$, for $R = 0$, 5, 10, 20, and ∞: (a) $\rho = 1$ and (b) $\rho = 0.1$.

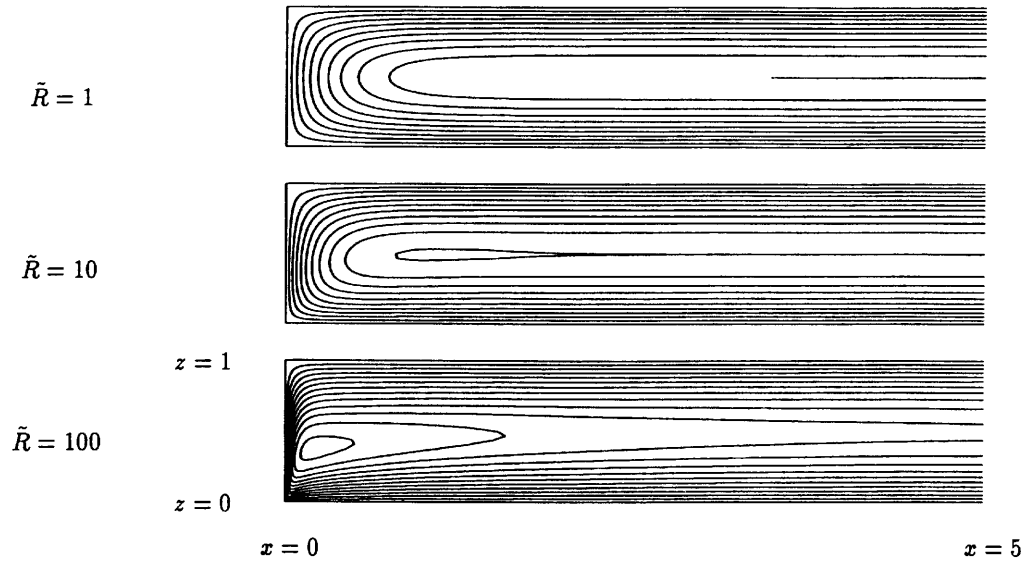


**Figure 5.** Contours of $\psi_0$ for various values of $\tilde{R}$ in the hot end region. Streamlines are plotted at an interval of 0.0125.

to one by this transformation, and because $f'(0)$ is always negative, $\tilde{R}$ and $R$ will have the same sign. The numerical solution of Eqs. (80) and (81) were performed using a time-dependent code and were integrated to steady state, using a slightly modified version of the finite difference code described in Rees and Bassom (1993). Briefly, the method used a first-order-accurate, backward-difference in time, and second-order-accurate, central-differences in space. The basic iteration scheme used was a pointwise Gauss-Seidel method with the Full Approximation Scheme multigrid algorithm; further details of the method may be found in Rees and Bassom (1993). The full numerical solution requires that the function $f(\hat{x})$ is known, and hence, that the value of $f'(0)$ is known, but this will be determined when solving the $O(A^2)$ core equations, later in the text. The value of $g(0)$ may be found from the detailed numerical solution.

## Core Solutions at $O(A^2)$

To determine $f(\hat{x})$, we need to solve the governing equation for $\hat{\theta}_2$, which may be given by

$$\frac{\partial^2\hat{\theta}_2}{\partial z^2} + f'' + \frac{f'}{\rho + \hat{x}} = -R^2\left(f'' + \frac{f'}{\rho + \hat{x}}\right) \cdot f'f'\left(\frac{z^4 - 2z^3 + z^2}{4}\right) + R^2 f'f'f'' \cdot\left(\frac{5}{12}z^4 - \frac{5}{6}z^3 + \frac{1}{4}z^2 + \frac{1}{6}z - \frac{7}{120}\right) + Rf'g'(2z - 1) \tag{85}$$

Integration once with respect to $z$ and the application of the boundary conditions at $z = 0$ and 1 gives the following equation:

$$f''\left(1 + \frac{R^2}{40}f'f'\right) + \frac{f'}{\rho + \hat{x}} \cdot\left(1 + \frac{R^2}{120}f'f'\right) = 0 \tag{86}$$

This nonlinear differential equation, subject to the boundary conditions [Eq. (70)], has been solved numerically, using a fourth-order Runge-Kutta scheme allied with the shooting method. Values of $f'(0)$ and $f'(1)$ are presented in Tables 1 and 2, respectively, for different values of $\rho$ and $R$. When $R \ll 1$, Eq. (86) reduces to Eq. (43). However, when $R$ is large, the leading-order form of the solution is given by

$$f = \frac{(\rho + 1)^{2/3} - (\rho + \hat{x})^{2/3}}{(\rho + 1)^{2/3} - \rho^{2/3}} + O(R^{-2}) \tag{87}$$

In Fig. 4, we display the form of $f(\hat{x})$ for selected values of $R$ and $\rho$. It is clear that, as $R$ increases, the profile of $f(\hat{x})$ varies monotonically between the ex-

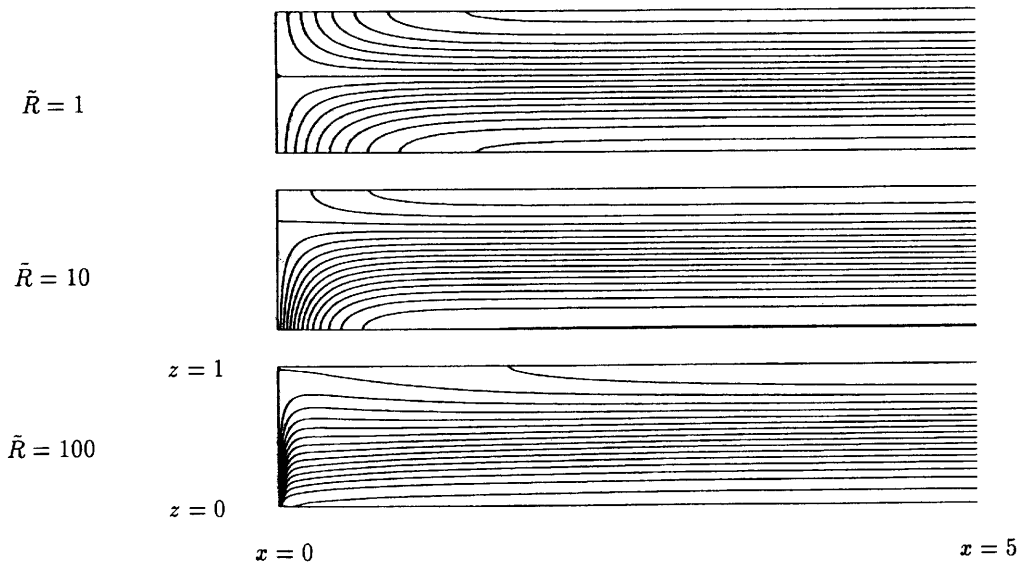


**Figure 6.** Contours of $\tilde{\theta}_1$ for various values of $\tilde{R}$ in the hot end region. Isotherms are plotted at an interval of $0.005\tilde{R}$.

tremes represented by $R = 0$ and $R = \infty$ analytical profiles, given by Eqs. (44) and (69), respectively. When $\rho$ takes relatively small values, the slope of $f(\hat{x})$ near the inner wall is relatively large, reflecting the fact that the heat is transferred into the core over a very small area compared with that of the outer wall.

Having obtained solutions for $f(\hat{x})$, and, in particular, the values of its derivatives at $\hat{x} = 0$ and 1, we now have all of the information necessary to solve Eqs. (80) and (81). Steady solutions in the form of streamlines are presented in Fig. 5 for a variety of values of $\tilde{R}$ and $\rho$. As $R$ is increased, the symmetric turning flow in the corners becomes increasingly asymmetrical, and eventually a distinct boundary-layer flow forms up the hot endwall. In the range of $\tilde{R}$ values presented in Fig. 5, the flow always tended to the steady state; it is possible that unsteady behavior might ensue if $\tilde{R}$ is sufficiently large as the governing equations are nonlinear. The corresponding $O(A^{-1})$ isotherms are displayed in Fig. 6. Again, the formation of the boundary layer at the vertical sidewall is evident as $\tilde{R}$ increases.

## RATE OF HEAT TRANSFER

In this section, we complete the analysis of the paper by determining the rates of heat transfer across the annulus for both asymptotic regimes, $Ra = O(1)$ and $Ra = O(A^{-1})$. The dimensional rate of heat transfer across any cylindrical surface, which is concentric with the inner and outer vertical surfaces of the annulus, is given by

$$Q = \int_0^h 2\pi\bar{r}\left[-k\frac{\partial T}{\partial \bar{r}} + \rho^* C_{\bar{p}}\bar{u}(T - T_c)\right] d\bar{z} \tag{88a}$$

When translated into nondimensional terms, Eq. (88a) may be expressed in the following form:

*Table 3*

*Values of Nu for various values of R and $\rho$*

| $R$ | $\rho = 0.01$ | $\rho = 0.1$ | $\rho = 1$ | $\rho = 10$ |
|---|---|---|---|---|
| 0 | 0.2171 | 0.4170 | 1.4427 | 10.492 |
| 1 | 0.2498 | 0.4283 | 1.4562 | 10.580 |
| 2 | 0.2869 | 0.4546 | 1.4960 | 10.834 |
| 5 | 0.3971 | 0.5748 | 1.7633 | 12.680 |
| 10 | 0.6361 | 0.8977 | 2.6844 | 19.242 |
| 20 | 1.4825 | 2.1090 | 6.3413 | 45.482 |
| 50 | 7.3494 | 10.548 | 31.923 | 229.11 |
| 100 | 28.300 | 40.686 | 123.30 | 885.17 |
| 200 | 112.10 | 161.23 | 488.77 | 3509.2 |
| 500 | 698.69 | 1005.04 | 3047.3 | 21872. |
| 1000 | 2793.6 | 4018.9 | 12186. | 87459. |

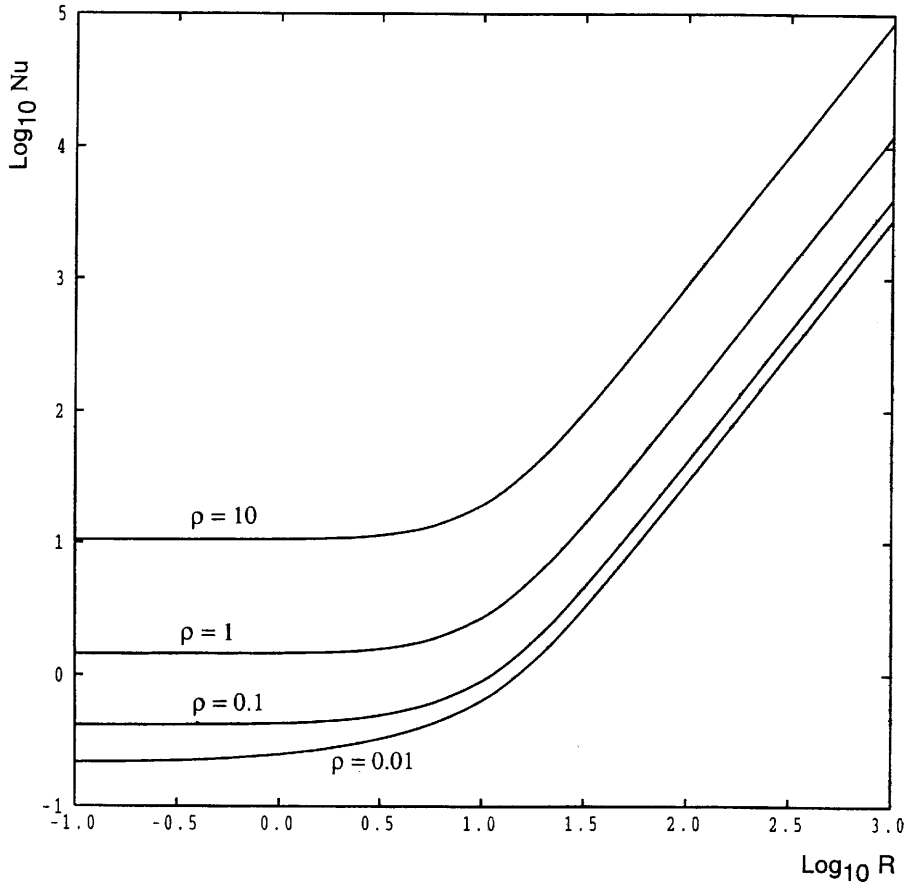


**Figure 7.** Variation of $Nu$ as a function of both $R$ and $\rho$.

$$Q = 2\pi kh(T_h - T_c) \cdot \int_0^1 \left[ -(\rho + \hat{x}) \frac{\partial \hat{\theta}}{\partial \hat{x}} - Ra\hat{\theta} \frac{\partial \tilde{\psi}}{\partial z} \right] dz \qquad (88b)$$

If we define $Nu$ to be the integral in Eq. (88b), then

$$Q = 2\pi kh(T_h - T_c)Nu \qquad (88c)$$

When $Ra = O(1)$, we can use the solutions derived in the Asymptotic Analysis for $Ra = O(1)$ section, to show that

$$Nu = -a + \frac{a^4(2\rho + 1)Ra^2A^2}{240\rho^2(\rho + 1)^2} + o(A^2) \qquad (89)$$

where we recall that $a = \{\ln[\rho/(\rho + 1)]\}^{-1}$ is negative, and hence, the leading term in $Nu$ is positive. The $O(A^2)$ correction to the leading-order Nusselt number is also positive, reflecting the increased rate of heat transfer that occurs as $Ra$ is increased. We note that the integral in Eq. (88b) has been evaluated at an arbitrary value of $\hat{x}$, but that the final result in Eq. (89) is independent of $\hat{x}$, as should be expected from a physical point of view.

When $Ra = O(A^{-1})$, the analysis of the Asymptotic Analysis for $Ra = O(A^{-1})$ section yields the following leading-order expression for the Nusselt number:

$$Nu = -(\rho + \hat{x}) f'(\hat{x}) \left\{ 1 + \frac{[Rf'(\hat{x})]^2}{120} \right\} + O(A) \qquad (90)$$

As it stands, Eq. (90) appears as if $Nu$ is a function of $\hat{x}$, which is physically unreasonable. However, if we multiply Eq. (86) by $(\rho + \hat{x})$, it becomes an exact differential and takes the following form:

$$\frac{dNu}{d\hat{x}} = 0 \qquad (91)$$

from which we deduce that $Nu$ is a constant. Values of $Nu$ for different values of $R$ and $\rho$ are presented in Table 3. It may be seen that the Nusselt number in-

creases as $R$ increases. The contents of Table 3 are also displayed in Fig. 7, where we see that there is a fairly sharp transition between a low-$R$ behavior, where $Nu$ is roughly constant, and a large-$R$ behavior, where $Nu$ is proportional to $R^2$. When $R$ is large, we can use Eq. (87) to show that the limiting form of $Nu$ is

$$Nu \sim \frac{R^2}{405[(\rho + 1)^{2/3} - \rho^{2/3}]^3} \tag{92}$$

## CONCLUSIONS

In this paper, we extended many earlier studies of flow in porous annuli subject to a radial flow of heat by considering the case of a very shallow annulus. Using the method of matched asymptotic expansions, we found that many of the important features of the flow, such as the parallel core flow at leading-order, higher-order corrections to the core flow, and the leading-order end-region flows, may be described analytically. Moreover, these solutions are valid at any fixed Rayleigh number, irrespective of its size, in the limit of small aspect ratios. For this range of values of the Rayleigh number, the flow is essentially dominated by the leading-order thermal conduction profile. The work was extended further by considering also the case when the Rayleigh number is asymptotically large, and in particular, we considered the case where $Ra = O(A^{-1})$ as $A \to 0$. In terms of the rescaled Rayleigh number, $R = RaA$, we found that increasing values of $R$ modify both the core conduction profile and the end-region flowfield. At large values of $R$, we find that boundary layers are formed on the heated surfaces, which is usually the case at large $O(1)$ values of $Ra$ in $O(1)$ aspect ratio cavities. Detailed heat transfer results have been presented for both asymptotic regimes.

We have assumed that the flow is axisymmetric. There are, of course, various circumstances where this assumption may not be true. One example is provided by a porous medium with either an anisotropic permeability, or an anisotropic diffusivity, or both. A second example is where the flow admits instabilities, although we do not think that that will happen for the present problem. In the core of the annulus, the flow is stably stratified and, therefore, instability, should it arise, will be induced in the thermal boundary layers in the end-regions. However, a recent pair of papers by Rees (1993) and Lewis et al. (1995) have shown that vertical thermal boundary layers from isothermal surfaces, such as occur in the present problem, are stable.

Although we have considered convection in a very shallow annulus with an asymptotically small aspect ratio, there are no experimental results against which our results can be compared.

## REFERENCES


Bejan, A., *Convection Heat Transfer*, Wiley, New York, 1984.

Bejan, A., Convective heat transfer in porous media, In: *Handbook of Single-Phase Convective Heat Transfer*, edited by S. Kakac, R. K. Shah, and W. Aung, Wiley, New York, 1987.

Brandt, A., Multigrid Techniques: 1984 Guide with Applications to Fluid Dynamics, Von Kármán Institute for Fluid Dynamics, Lecture Series 1984-04, 1984.

Dharma Rao, V., Naidu, S. V., and Sarma, P. K., Non-Darcy effects in natural convection heat transfer in a vertical porous annulus, *Trans. ASME J. Heat Transfer*, vol. 118, pp. 502–505, 1996.

Havstad, M. A. and Burns, P. J., Convective heat transfer in vertical cylindrical annuli filled with a porous medium, *Int. J. Heat Mass Transf.*, vol. 25, pp. 1755–1766, 1982.

Hickox, C. E. and Gartling, D. K., A numerical study of natural convection in a vertical, annular, porous layer, *Int. J. Heat Mass Transf.*, vol. 28, pp. 720–723, 1985.

Lewis, S., Bassom, A. P., and Rees, D. A. S., The stability of vertical thermal boundary layer flow in a porous medium, *European Journal of Mechanics B: Fluids*, vol. 14, pp. 395–408, 1995.

Merker, G. P. and Leal, L. G., Natural convection in a shallow annular cavity, *Int. J. Heat Mass Transf.*, vol. 23, pp. 677–686, 1980.

Nield, D. A. and Bejan, A., *Convection in Porous Media*, Springer-Verlag, New York, 1992.

Prasad, V. and Kulacki, F. A., Natural convection in a vertical porous annulus, *Int. J. Heat Mass Transf.*, vol. 27, pp. 209–219, 1984.

Prasad, V. and Kulacki, F. A., Natural convection in porous media bounded by short concentric vertical cylinders, *Trans. ASME J. Heat Transf.*, vol. 107, pp. 147–154, 1985.

Prasad, V., Kulacki, F. A., and Kulkarni, A. V., Free convection in a vertical, porous annulus with constant heat flux on the inner wall—experimental results, *Int. J. Heat*

*Mass Transf.*, vol. 29, pp. 713–723, 1986.

Rao, Y. F. and Wang, B. X., Natural convection in vertical porous enclosures with internal heat generation, *Int. J. Heat Mass Transf.*, vol. 34, pp. 247–252, 1991.

Rees, D. A. S., Nonlinear wave stability of vertical thermal boundary layer flow in a porous medium, *Journal of Applied Mathematics and Physics (Z.A.M.P.)*, vol. 44, pp. 306–313, 1993.

Rees, D. A. S. and Bassom A. P., The nonlinear nonparallel wave instability of free convection induced by a horizontal heated surface in fluid-saturated porous media, *J. Fluid Mech.*, vol. 253, pp. 267–296, 1993.